


Article

A Novel Trace-Level Ammonia Gas Sensing Based on Flexible PANi-CoFe₂O₄ Nanocomposite Film at Room Temperature

Rima D. Alharthy¹ and Ahmed Saleh^{2,*} 

¹ Department of Chemistry, Science and Arts College, Rabigh Campus, King Abdulaziz University, Jeddah 21577, Saudi Arabia; iaaalharte@kau.edu.sa

² Science and Technology Center of Excellence (STCE), Cairo 3066, Egypt

* Correspondence: mr_asaleh1@yahoo.com or asaleh@stce-egypt.org

Abstract: In this study, we developed a new chemi-resistive, flexible and selective ammonia (NH₃) gas sensor. The sensor was prepared by depositing thin film of polyaniline-cobalt ferrite (PANi-CoFe₂O₄) nanocomposite on flexible polyethylene terephthalate (PET) through an in situ chemical oxidative polymerization method. The prepared PANi-CoFe₂O₄ nanocomposite and flexible PET-PANi-CoFe₂O₄ sensor were evaluated for their thermal stability, surface morphology and materials composition. The response to NH₃ gas of the developed sensor was examined thoroughly in the range of 1–50 ppm at room temperature. The sensor with 50 wt% CoFe₂O₄ NPs content showed an optimum selectivity to NH₃ molecules, with a 118.3% response towards 50 ppm in 24.3 s response time. Furthermore, the sensor showed good reproducibility, ultra-low detection limit (25 ppb) and excellent flexibility. In addition, the relative humidity effect on the sensor performance was investigated. Consequently, the flexible PET-PANi-CoFe₂O₄ sensor is a promising candidate for trace-level on-site sensing of NH₃ in wearable electronic or portable devices.

Keywords: polyaniline; cobalt ferrite; ammonia gas sensor; flexible; nanocomposite



Citation: Alharthy, R.D.; Saleh, A. A Novel Trace-Level Ammonia Gas Sensing Based on Flexible PANi-CoFe₂O₄ Nanocomposite Film at Room Temperature. *Polymers* **2021**, *13*, 3077. <https://doi.org/10.3390/polym13183077>

Academic Editors: Amor M. Abdelkader, Mohamed Shafick Zoromba, Mohamed Helmy Abdel-Aziz and Numan Salah

Received: 21 August 2021
Accepted: 9 September 2021
Published: 12 September 2021

Publisher's Note: MDPI stays neutral with regard to jurisdictional claims in published maps and institutional affiliations.



Copyright: © 2021 by the authors. Licensee MDPI, Basel, Switzerland. This article is an open access article distributed under the terms and conditions of the Creative Commons Attribution (CC BY) license (<https://creativecommons.org/licenses/by/4.0/>).

1. Introduction

Ammonia (NH₃) is a pungent, toxic, colorless, water-soluble and flammable gas produced worldwide in large quantities of more than 200 million tons per annum. It plays a vital role in all life forms and is one of the major industrial raw materials in chemicals production facilities such as agriculture, refrigeration technology, food, fertilizers and medical facilities [1,2]. According to Occupational Safety and Health Administration (OSHA) and the Agency for Toxic Substances and Disease Registry (ATSDR), ammonia is hazardous gas and its presence in atmosphere even at very low concentrations of 50 ppm could irritate the respiratory tract, skin, nose and throat of children and/or adults. It also has a bad impact on the environment and can cause lung damage or even death at high concentration levels beyond 500 ppm [3]. Therefore, a low-cost, sensitive, stable, ambient temperature, and reliable ammonia detection sensor is imperative. Recently, conductive conjugated polymers on flexible substrate are in fashion as sensing materials for trace-level detection of ammonia owing to their lightweight, flexible, and portable nature [4]. These type of ammonia sensors are widely reported due to their simple synthesis, ambient temperature sensitivity and low cost processing [5–8]. In this context, polyaniline (PANi) is one of the most significant conducting polymers used for ammonia sensing because of its high reactivity and facile synthesis [9] along with its reversible doping/dedoping property [10], excellent electrical properties, unique redox characteristics and adjustable sensing at ambient temperature. However, pure PANi-based sensors have certain associated caveats, such as limited sensing efficiency in context of response, selectivity, and long response/recovery time [11]. Recently, researchers focused more on PANi-based nanocomposites using functionalized carbon-based materials and metal oxide semiconductors [12–17] that resulted in a significant performance improvement in PANi-based ammonia sensors.

The current tendency in producing trace-level NH_3 gas sensors is to prepare flexible substrate sensors based on PANi as conducting polymers due to their lightweight, portable, and flexible properties. Y. Zhang et al. [18] prepared an NH_3 sensor based on polyaniline/ SrGe_4O_9 nanocomposite on Polyimide (PI) substrate by in situ chemical oxidation polymerization technique. The sensor revealed excellent response time (24 s), good flexibility and reproducibility. Q. Wu et al. [4] utilized porous polyvinylidene fluoride (PVDF) as a flexible template for PANi composed with graphene (GP) with 10% response towards 0.1 ppm NH_3 and response time (46 s). J. Ma et al. [19] modified PET fibers by ethylenediamine (EDA) to expose amino groups and adhere to carboxyl groups of MWCNTs and coated by PANi, the sensor showed 117% response towards 50 ppm NH_3 with response time (47 s) and cost-effective flexible substrate modification.

Cobalt ferrite (CoFe_2O_4) is an n-type semiconductor with band gap of 1.76 eV [20]. This material showed promising magnetization properties [21,22], including high remanence magnetization and coercivity. It also has shown high chemical stability, cost-effectiveness, and shape versatility when produced at high temperatures. Cobalt ferrites have been applied in many technological fields, such as ferrofluids, catalysis, electronics, cancer treatment [23] and chemi-resistive sensors [24]. It has an inverse spinel structure in which, Fe^{3+} ions are distributed between octahedral and tetrahedral sites and Co^{2+} ions are in octahedral sites. In oxidation reactions, CoFe_2O_4 has significant catalytic properties due to the high mobility of oxygen ion at the film surface and thus is highly preferred for the gas sensing applications [25].

Herein, we report a thin film of PANi- CoFe_2O_4 nanocomposites with different concentrations of CoFe_2O_4 NPs deposited on a flexible PET substrate by using in situ chemical oxidative polymerization technique. The prepared sensor is subsequently applied for room temperature detection NH_3 gas. Several gas sensing parameters, such as selectivity, response at different gas concentrations, reproducibility, response/recovery times, flexibility, and low detection limit were studied.

2. Experimental

2.1. Materials

Cobalt (II) nitrate hexahydrate [$\text{Co}(\text{NO}_3)_2 \cdot 6\text{H}_2\text{O}$, $\geq 99\%$ Fluka, Germany], Iron(III) nitrate nonahydrate ($\text{Fe}(\text{NO}_3)_3 \cdot 9\text{H}_2\text{O}$, $\geq 98\%$, from Sigma-Aldrich), citric acid as fuel (99.6%, Acros), Aniline monomer ($\text{C}_6\text{H}_7\text{N}$, Merck, Germany, 99.5%), ammonium persulfate, APS ($(\text{NH}_4)_2\text{S}_2\text{O}_8$, Acros, Belgium, 98%) as an oxidant, hydrochloric acid (37%) and ammonia solution (35%) (Fisher Scientific, Belgium) were used as received. Polyethylene terephthalate (PET) film with dimensions of 7 cm \times 3 cm with ± 80 μm thickness was used without any further treatment. DI water was used for the synthesis of CoFe_2O_4 NPs and the polyaniline nanocomposites.

2.2. Fabrication of Flexible PET-PANi- CoFe_2O_4 Sensor Films

CoFe_2O_4 nanoparticles (NPs) were prepared by sol-gel combustion technique as reported by L. E. Caldeira et al. [26] as following; ($\text{Co}(\text{NO}_3)_2 \cdot 6\text{H}_2\text{O}$), ($\text{Fe}(\text{NO}_3)_3 \cdot 9\text{H}_2\text{O}$) and citric acid were dissolved in 20 mL DI with 1:2:3 molar ratio. The mixture was stirred and heated at 85 $^\circ\text{C}$ for 1 h. The gel was dried for 24 h at 110 $^\circ\text{C}$ to remove the water. The xerogel was sintered in muffle furnace for 6 h at 750 $^\circ\text{C}$. In situ chemical oxidative polymerization technique was used to prepare PANi- CoFe_2O_4 nanocomposite films on flexible PET substrates by polymerization of $\text{C}_6\text{H}_7\text{N}$ monomer in dilute hydrochloric acid using $(\text{NH}_4)_2\text{S}_2\text{O}_8$ as an oxidant. The method leads to the deposition of PANi- CoFe_2O_4 thin film on flexible substrate (in this work, PET). Before use, the PET films were cleaned by immersing in boiling acetone and then in isopropyl alcohol followed by drying for 1 h at 70 $^\circ\text{C}$. The experimental procedure is as follows: PET films were immersed vertically in solution of 0.2 M $\text{C}_6\text{H}_7\text{N}$ monomer dissolved in 1 M HCl at 0–5 $^\circ\text{C}$. The mixture was stirred using a mechanical stirrer supplied with Teflon rod to avoid any agglomeration. After ~ 1 h, 0.1 M $(\text{NH}_4)_2\text{S}_2\text{O}_8$ was drop-wise added to the above mixture with continuous stirring

and kept at these conditions for further 14 h. Finally, a green emeraldine salt precipitate of PANi was formed. The as-synthesized CoFe_2O_4 NPs (10, 30 and 50 wt%) were sonicated and added to the $\text{C}_6\text{H}_7\text{N}$ for the preparation of hybrid nanocomposite on the PET film. The flexible film was filtered from the PANi solution, washed with DI water and finally placed in an oven at 60°C for 1 h. The screen-printing technique was used to print the silver-integrated electrode onto the surface of the film to obtain the flexible gas sensor film. The scheme of film formation is depicted in Figure 1.

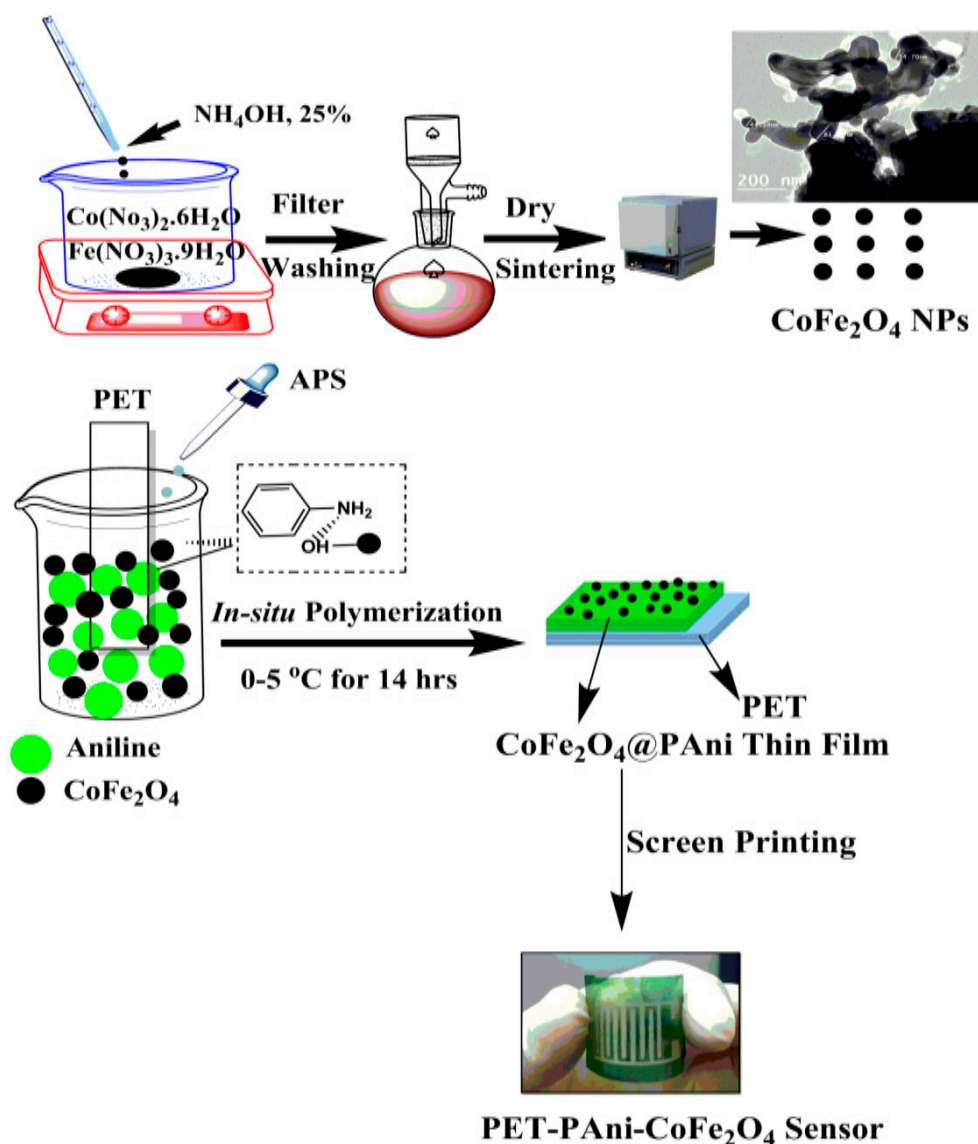


Figure 1. Flexible PET-PAni- CoFe_2O_4 nanocomposite film formation.

2.3. Characterization and Gas Detection Measurements

As-prepared samples were investigated for their chemical structure by Fourier transform infrared spectroscopy (FT-IR) (Thermo Nicolet Avatar 370). Structural study was conducted by XRD (ARL X'TRA Powder Diffractometer, Thermo Scientific) at a speed of 5° per min, 2θ scan range $5-80^\circ$ with λ 1.5406 Å. Surface topography and surface roughness average (Ra) for flexible sensors were measured by a profilometer with contact stylus tracing (KLA Tencor™ P-7, Milpitas, California, USA). The diameter of the diamond tip was 2.4 mm with accuracy 1 mm/s. Measurements were performed in three different positions of each film, Ra Mean values were calculated for each sample. The surface morphology was carried out by FE-SEM (Quanta FEG 250, Waltham, MA, USA). CoFe_2O_4 particle size

was investigated using HR-TEM (JEOL-2100, Tokyo, Japan). The glass transitions (T_g) of the flexible sensors were carried out using a (TA Instruments DSC Q4000, New Castle, DE, USA). The thermal stability of samples was monitored by TGA using a (TA Instrument TGA Q500, New Castle, DE, USA) with nitrogen purge flow 50 mL per min at 25–900 °C with a ramp rate of 10 °C per min. PANi-CoFe₂O₄ (50%) nanocomposite elemental composition was evaluated by XPS (K-ALPHA, Thermo Fisher Scientific, Waltham, MA, USA). CoFe₂O₄ NPs hysteresis loop parameters were evaluated by a Vibrating Sample Magnetometer (VSM) (Lakeshore-7410, Westerville, OH, USA). The gas sensing properties of the sensors were evaluated at 40% relative humidity and room temperature by a homemade chamber as shown in Figure 2. The chamber is attached with a real-time acquisition system to measure the resistance. Prior to introducing NH₃ gas in to the test chamber, the sensor film was stabilized for 20 min to obtain the stable baseline in dry air, then a gas stream in the ambient temperature with various concentrations in the range of 1–50 ppm was injected to evaluate the sensors responses NH₃ and selectivity test of interfering gas molecules (CO₂, C₂H₅OH and CH₃OH) at 50 ppm. A mass flow controller (MFC 300) (was utilized to expose a constant flux of 50 cm³ min⁻¹ from dry air to various injected target gas). To desorb NH₃ after each test, the sensor was flushed with dry air. The % response of the sensor is expressed by the following equation:

$$\text{Response (\%)} = \frac{R_g - R_o}{R_o} \times 100 \quad (1)$$

where R_o and R_g are the measured resistances of air and tested gas, respectively [27,28]. The recovery time (T_{rec}) and response time (T_{res}) were measured as the times taken by the film sensor to reach 90% of the resistance change [29,30]. The humidity effect on PET-PANi-CoFe₂O₄ sensor was detected using humidity chamber (Cincinnati Sub Zero—CSZ) by replacing the test gas chamber in the environmental chamber and adjusting the desired value of RH for 20 min till equilibrium before testing.

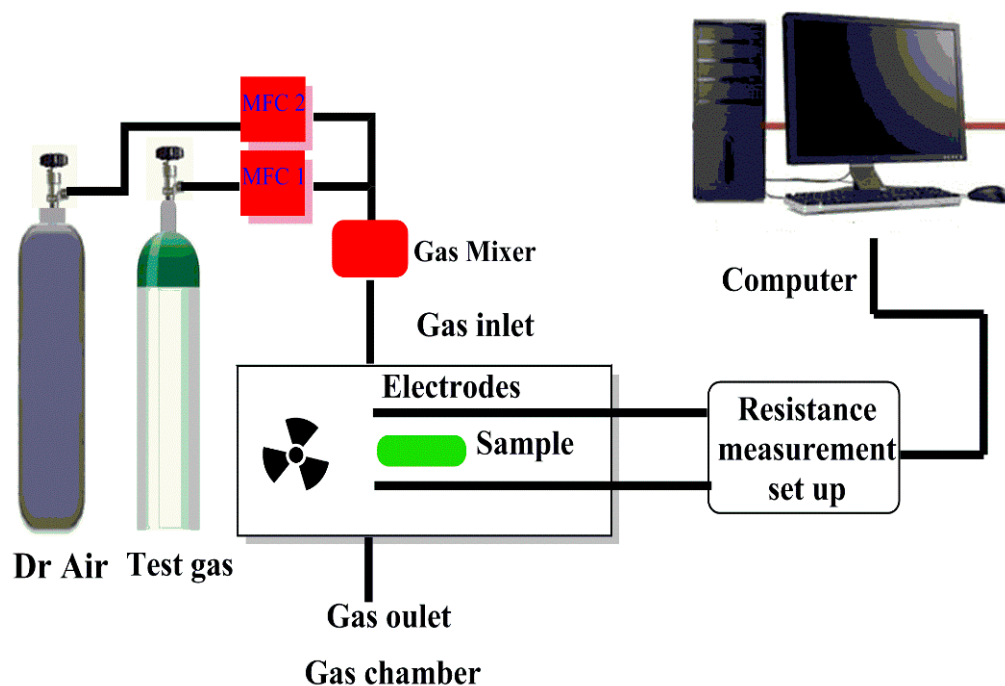


Figure 2. The gas sensing setup diagram.

3. Results and Discussion

3.1. Magnetic Properties of CoFe_2O_4 NPs

The calcination temperature effect on the magnetic parameters of the precursor was recorded by VSM at room temperature, Figure 3 displays the M-H hysteresis loop for the CoFe_2O_4 NPs. The hysteresis curve shows ferrimagnetic performance of spinel CoFe_2O_4 nanocrystals. The coercive field (H_c), saturation magnetization (M_s), remanence magnetization (M_r), and the squareness (R) value (M_r/M_s), were 1523 (Oe), 68.5 (emu/g), 29.5 (emu/g), and 0.43, respectively. The value of M_s is lower than the observed bulk (74.08 emu/g) [31]; this may be attributed to the modified cationic distribution and the disorder of the nanoparticle's surface. This is an indication of the excellent magnetic properties of CoFe_2O_4 .

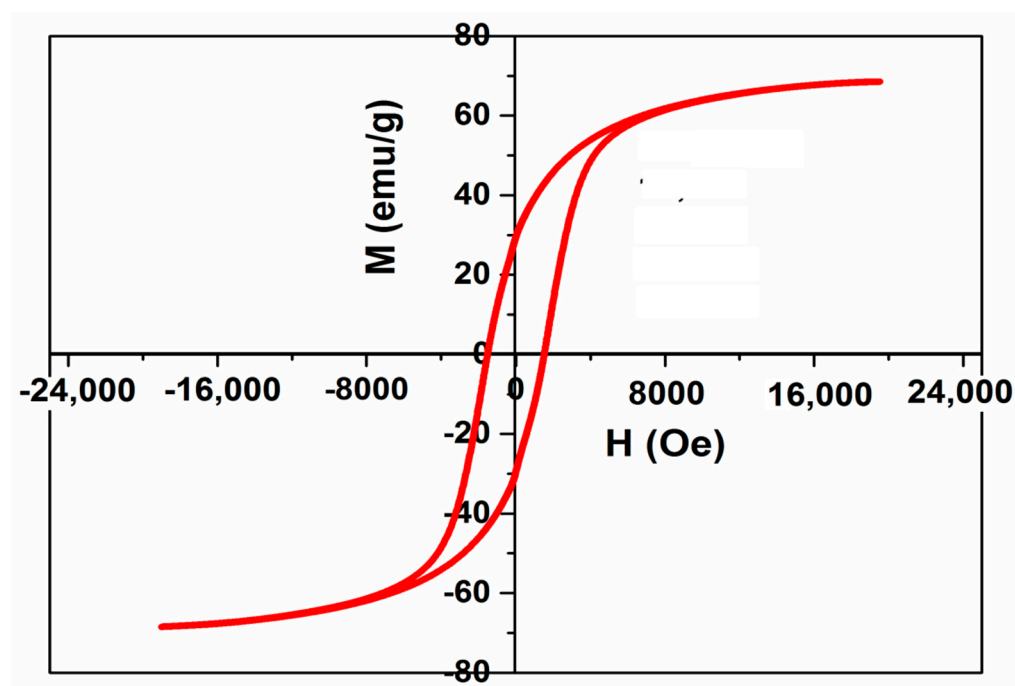


Figure 3. Hysteresis loop of CoFe_2O_4 sample.

3.2. FT-IR Analysis

FT-IR spectra of PANi, CoFe_2O_4 NPs, and PANi- CoFe_2O_4 (50%) nanocomposite are presented in Figure 4. The spectrum of PANi have a peak at 797 cm^{-1} due to C—H bending of aromatic ring (out of plane) [32]. The absorption peaks at 1131 cm^{-1} and 1293 cm^{-1} are attributed to the C—N stretching of quinoid and benzenoid ring, respectively [33]. The peaks at 1479 cm^{-1} and 1563 cm^{-1} represent the stretching vibration C=C of benzenoid and quinoid structure, respectively [34]. The peak observed at 2411 cm^{-1} is due to C=NH⁺ [35]. The PANi spectrum has a prominent peak at 3417 cm^{-1} for aromatic amine —N-H stretching while the peaks at 2919 and 2850 cm^{-1} are attributed to —C-H stretching. The above-mentioned typical peaks confirm the synthesis of PANi in protonated state. CoFe_2O_4 have strong peaks at 580 and 493 cm^{-1} which represent the vibrations (ν) of M-O (Metal (M)=Fe, Co) symmetric stretching in tetrahedral and octahedral sites of CoFe_2O_4 [36,37]. The peak at 1633 cm^{-1} corresponds to bending vibration of H-O-H [23]. The peak at 3432 cm^{-1} can be inferred to stretching vibration of O-H group at the surface of NPs due to surface water [38]. It is important to note that that the peak of CoFe_2O_4 in the spectrum of PANi- CoFe_2O_4 (50%) nanocomposite shifted to higher wavenumbers of 584 cm^{-1} that indicates the strong interaction between metal ions of CoFe_2O_4 and nitrogen atoms of PANi due to hydrogen bonding.

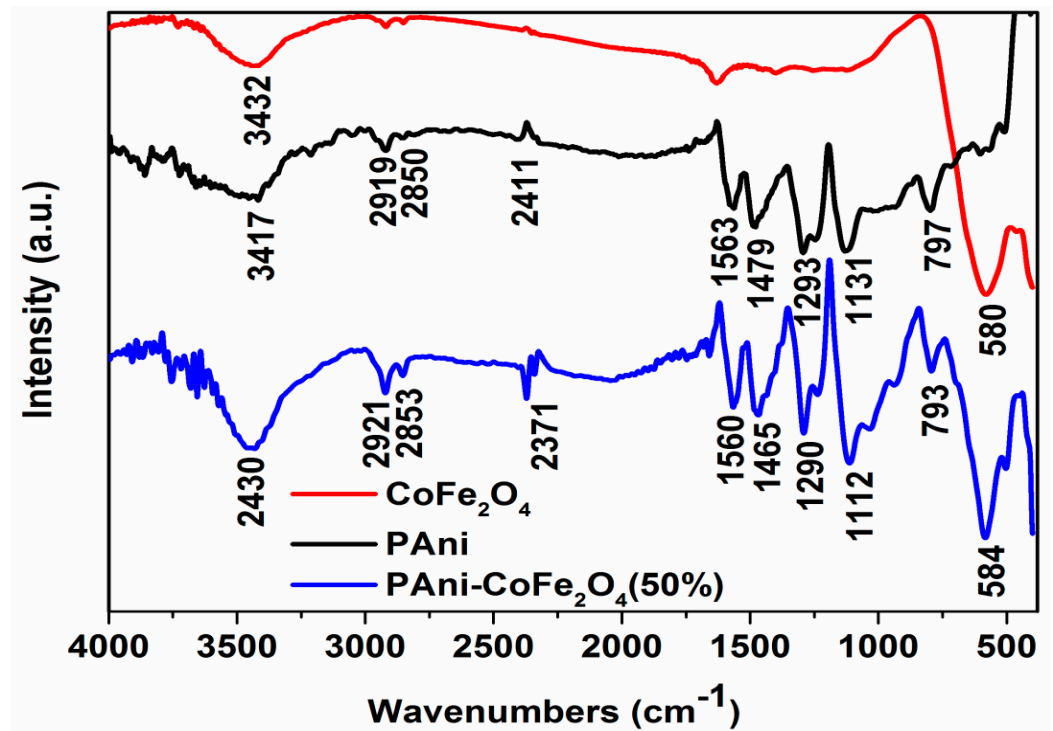


Figure 4. FT-IR of CoFe₂O₄, PANi and nanocomposite of PANi-CoFe₂O₄ (50%).

3.3. XRD Analysis

The XRD pattern of CoFe₂O₄ NPs, PANi and PANi-CoFe₂O₄ (50%) nanocomposite powder is presented in Figure 5. CoFe₂O₄ NPs showed reflection planes namely (220), (311), (222), (400), (422), (511) and (440). The observed peaks matched with (JCPDS 00-002-1045, space group Fd3m, space group number no 227) for reflections of cubic spinel structure. The the average crystallite size as obtained by the Scherrer formula was found to be 41 nm.

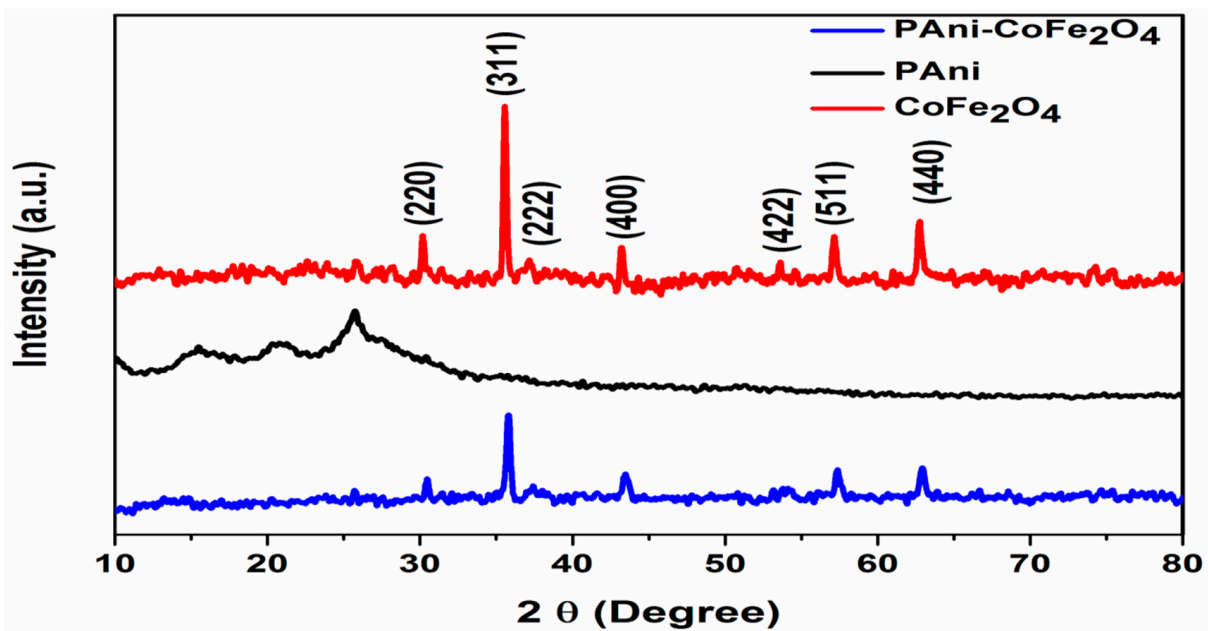


Figure 5. The XRD of CoFe₂O₄, PANi and nanocomposite of PANi-CoFe₂O₄ (50%).

For PANi, two broad peaks at 20 and 25° are related to the amorphous structure of PANi [39]. In PANi-CoFe₂O₄ (50%), no diffraction peak for PANi was noticed in the pattern, which confirms the amorphous nature of PANi in its composites with metal oxides [40]. In the composite synthesis, the ammonium persulfate as an oxidative initiator proceeded on the CoFe₂O₄ NPs surface and encapsulated in PANi shell leading to the resistive effect of nanoparticles that hamper the crystallinity of PANi. The crystal form of CoFe₂O₄ NPs in PANi-CoFe₂O₄ composite pattern showed low crystallinity compared to CoFe₂O₄; the phenomenon is attributed to the coating effect and intermolecular interaction between surface of CoFe₂O₄ and conducting PANi [41].

3.4. Morphological Analysis (FE-SEM)

FE-SEM analysis was performed to visualize the morphology of the as-synthesized CoFe₂O₄ NPs, PET-PANi and PET-PANi-CoFe₂O₄ (50%) sensors, Figure 6. According to the results of FE-SEMSEM, the CoFe₂O₄ NPs, Figure 6a, have a tendency to agglomerate that is attributed to their ferrimagnetic properties [42] and sponge-like structure with porous morphology, which may have a great impact on the sensing properties. Despite the agglomeration and the blurred edges of CoFe₂O₄, the NPs are still uniform spheres with particle sizes of 70–80 nm. The larger grain size might be attributed to crystallites magnetic properties.

A quantitative elemental EDS spectrum in Figure 6b is used to calculate the CoFe₂O₄ NPs composition, the molar ratio of Co, Fe, and O was found to be 1:1.96:3.94 that is fairly close to the theoretical values of 1:2:4, indicating the nominal composition and the stoichiometric proportion is maintained. It is clear from Figure 6c that PANi behaves in a similar way to a well-developed interconnected fiber with porous morphology in PET-PANi film. The surface morphology of PET-PANi-CoFe₂O₄ (50%) film was found in clusters, porous and rough surface, Figure 6d. Moreover, the agglomeration of CoFe₂O₄ NPs on the PANi surface was observed, which endorses literature reports showing that an increase in NPs loading in the matrix leads to coagulation [43].

3.5. TEM Analysis

TEM and SAED patterns were recorded for detailed insight into the microstructure of CoFe₂O₄ NPs (Figure 7). The particles have a spherical shape with particle size in the range of 40–80 nm (Figure 7a). Segregated as well as agglomerated particles are clearly visible which endorse FE-SEM data. Selected area electron diffraction (SAED) pattern shows white spot rings indicating the polycrystalline structure of CoFe₂O₄ NPs, Figure 7b. SAED results matched well with the XRD patterns.

3.6. Roughness Measurements

Profilometer is one of the most commonly used devices for measuring the roughness (Ra) and 3D images for the nanocomposite. Generally, the roughness of the nanocomposite surface depends on the structure of the organic matrix and the content of the inorganic filler. The surface topography of PET-PANi shows a relatively uniform and smooth structure compared to PET-PANi-CoFe₂O₄ (50%) in Figure 8. The mean surface roughness of the PET-PANi and PET-PANi-CoFe₂O₄ (50%) samples were found to be 1.15 and 5.3 μm, respectively. This increase in Ra value lead to augmented polarity and surface area that results in extra growth sites and buildup of adhesion between PANi and CoFe₂O₄ NPs.

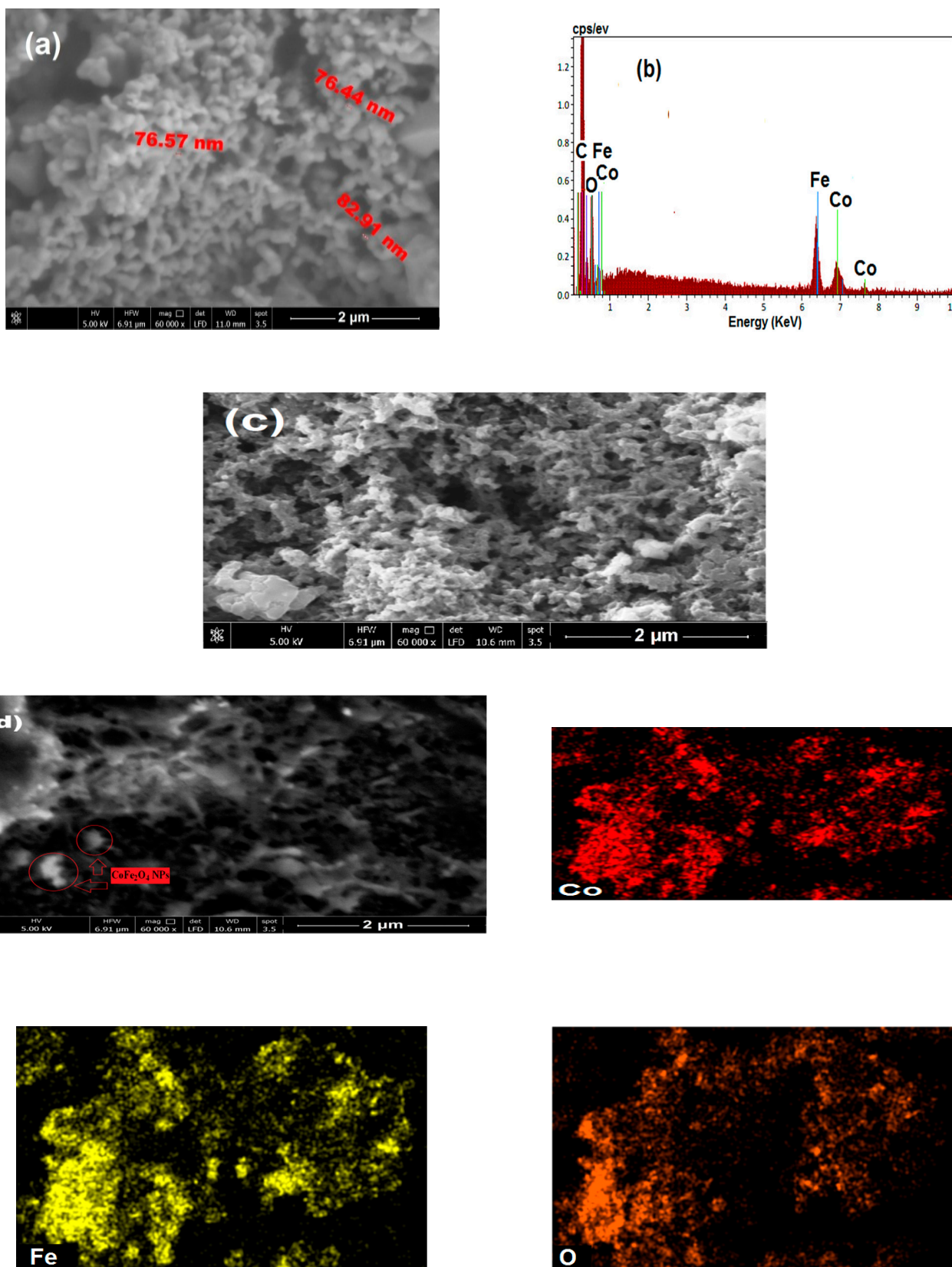


Figure 6. FE-SEM of (a) CoFe_2O_4 , (b) EDS of CoFe_2O_4 , (c) PET-PANI and (d) PET-PANI- CoFe_2O_4 (50%) sensor and its elemental mapping images of the Co (red), Fe (yellow) and O (brown) signals.

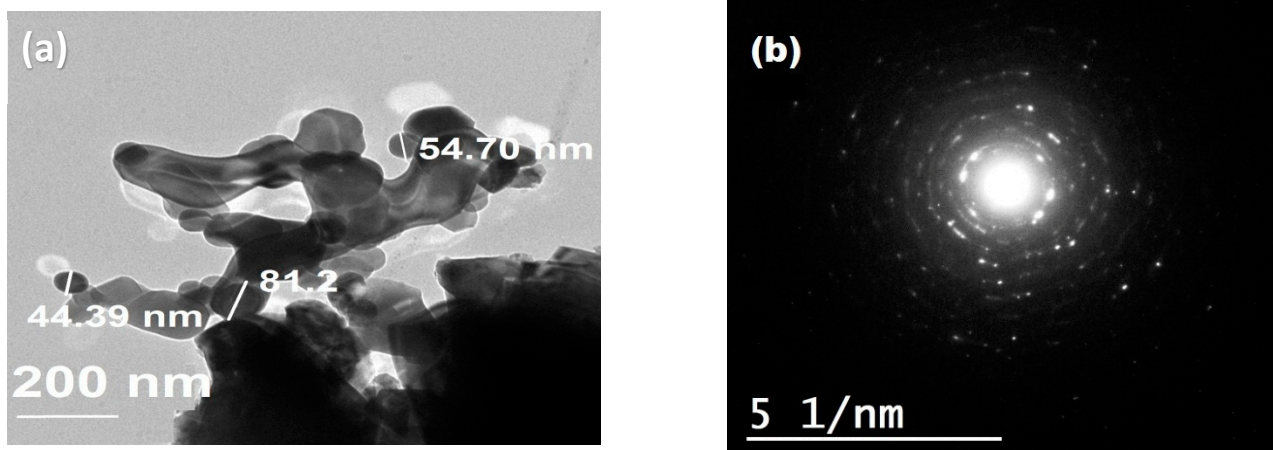


Figure 7. (a) TEM and (b) SAED pattern of CoFe_2O_4 .

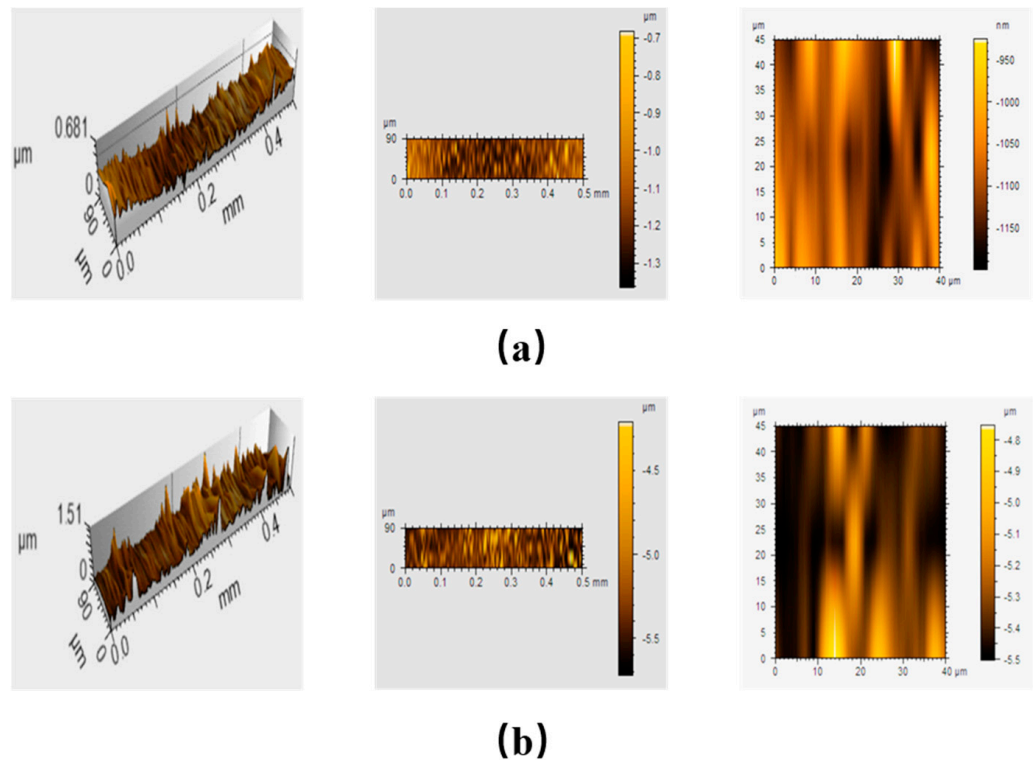


Figure 8. Surface structure images of (a) PET-PAni and (b) PET-PAni- CoFe_2O_4 (50%) measured by stylus profiler.

3.7. Thermal Analyses

3.7.1. Thermogravimetric Analysis (TGA)

TG and DTG thermograms of CoFe_2O_4 , PAni, PAni- CoFe_2O_4 (50%), PET, PET-PAni and PET-PAni- CoFe_2O_4 (50%) are shown in Figure 9a,b. The degradation of CoFe_2O_4 occurred in two stages having an insignificant loss: the first step was up to $600\text{ }^\circ\text{C}$ that is attributed to the loss of moisture, decarbonation and removal of hydroxyl group associated with the NPs (0.21%) while the second step at higher temperature was up to $900\text{ }^\circ\text{C}$ (0.18%) [44]. The TGA thermogram confirms the high thermal stability of CoFe_2O_4 NPs. For pure PAni, there are three main stages of pyrolysis, the first between 30 to $140\text{ }^\circ\text{C}$ that is attributed to loss of adsorbed water, unreacted monomer and free acid remaining after polymerization, 8.54% [45]. The second stage is found in a range of 140 to $325\text{ }^\circ\text{C}$ due to the degradation of low molecular weight oligomers formed during the synthesis of PAni,

11.49% and residue 7.73% [46]. The third and last stage was in a temperature range 350 to 900 °C due to the structural breakdown of PANi molecules, 69.3% degradation and residue 14.5% [47]. PANi-CoFe₂O₄ (50%) nanocomposite have shown the same thermal degradation behavior as PANi, as they have a somewhat high thermal stability with a residue (33.2%). Moreover, the thermal stability of plastic films coated with nanocomposite thin film was also examined. The TG curves reveal that the decomposition of PET substrate occurred in one step in a temperature range of 300–520 °C, related to the random degradation of ester groups into carbonyl and vinyl ester which were subsequent converted to acetaldehyde by tautomerization effect [48] with a weight loss of 94.86% and char residue of 5.15% at 900 °C. The PET-PAni film showed typical behavior of PET but with more weight loss of 96.4% and residue of 3.6%, which may be attributed to the catalytic effect of PANi during the decomposition of PET film. The PET film coated with PANi-CoFe₂O₄ (50%) showed higher thermal stability compared to all other films with weight loss of 92.7% and residue of 7.3% due to the high thermal stability of CoFe₂O₄ embedded in the PET film.

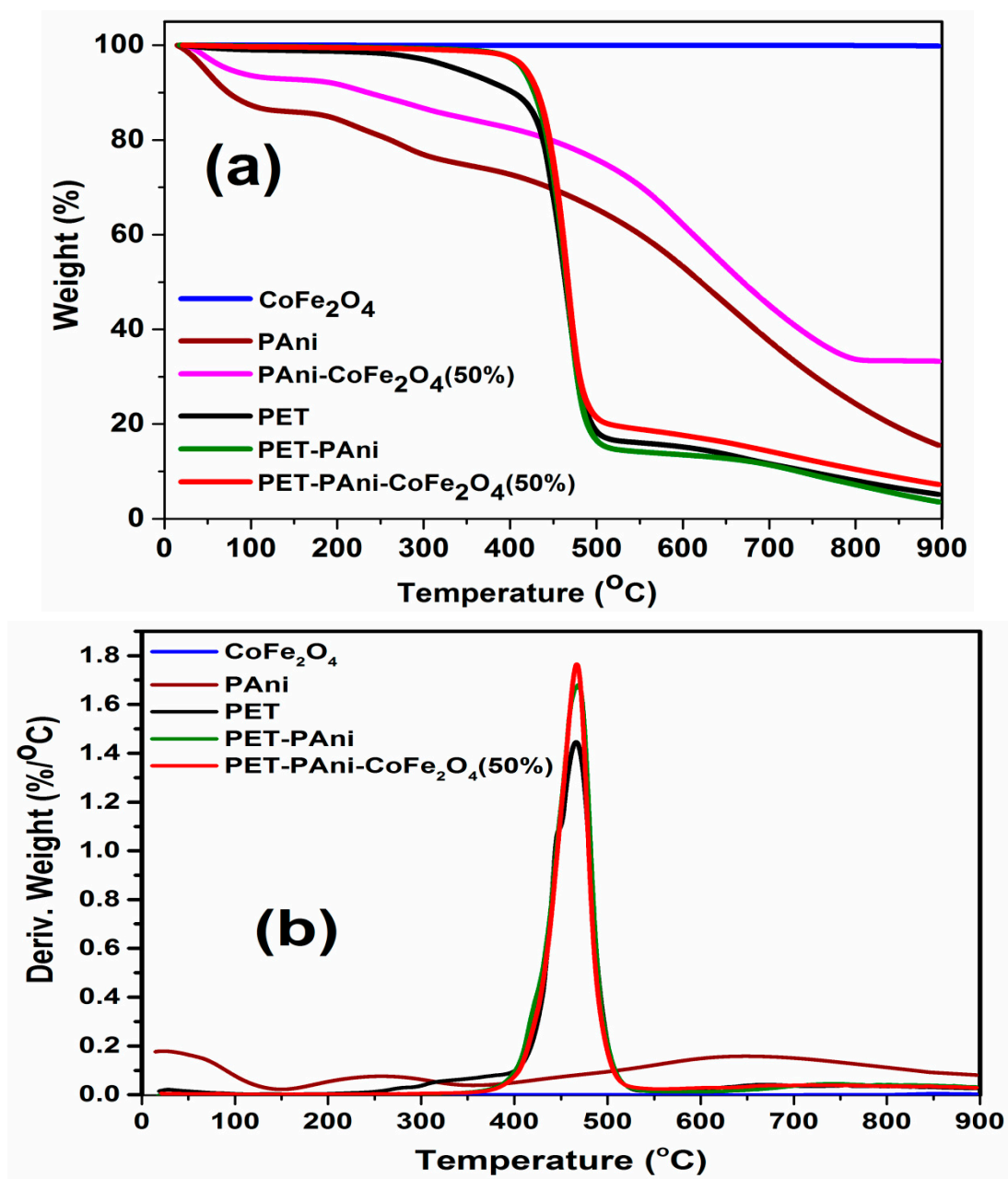


Figure 9. TG (a) and DTG curves (b) of CoFe₂O₄, PANi, PANi-CoFe₂O₄ (50%) nanocomposite, PET, PET-PAni and PET-PAni-CoFe₂O₄ (50%).

3.7.2. Differential Scanning Calorimetry (DSC)

The interactions of PET film with PANi and CoFe₂O₄ during the in situ polymerization reaction were monitored, which were responsible for the nanocomposite phase transitions (see Figure 10). One-step DSC scanning is performed from ambient conditions to 300 °C. The glass transition (*T_g*) of pristine PET, PET-PANi, and PET-PANi-CoFe₂O₄ (50%) were found to be 81 °C, 81.3 °C, and 82.7 °C, respectively. The slight increase in *T_g* may be attributed to the interaction between the PET substrate and nano-fillers that resulted in a reduction in the polymer segmental motion. To understand the effect of the coated nano-fillers on polymer structural characteristics, the polymer crystallinity was studied using the heat of fusion obtained from DSC thermograms and the degree of crystallinity, Xc%, was determined by using Equation (2) [49].

$$Xc\% = \frac{\Delta H}{\Delta H_0} \times 100 \quad (2)$$

where ΔH is the PET melting enthalpy and ΔH_0 is the 100% crystalline PET melting enthalpy, considered to be 140 Jg⁻¹ [50]. The PET crystallinity degree was found to be 30.6%, which shifted to higher values for PET-PANi and PET-PANi-CoFe₂O₄ (50%) to 32.5% and 35.7%, respectively. This increase in crystallinity may be attributed to the creation of segments of small chains, which are capable of crystallization and realigning easily, as indicated by TGA and FT-IR.

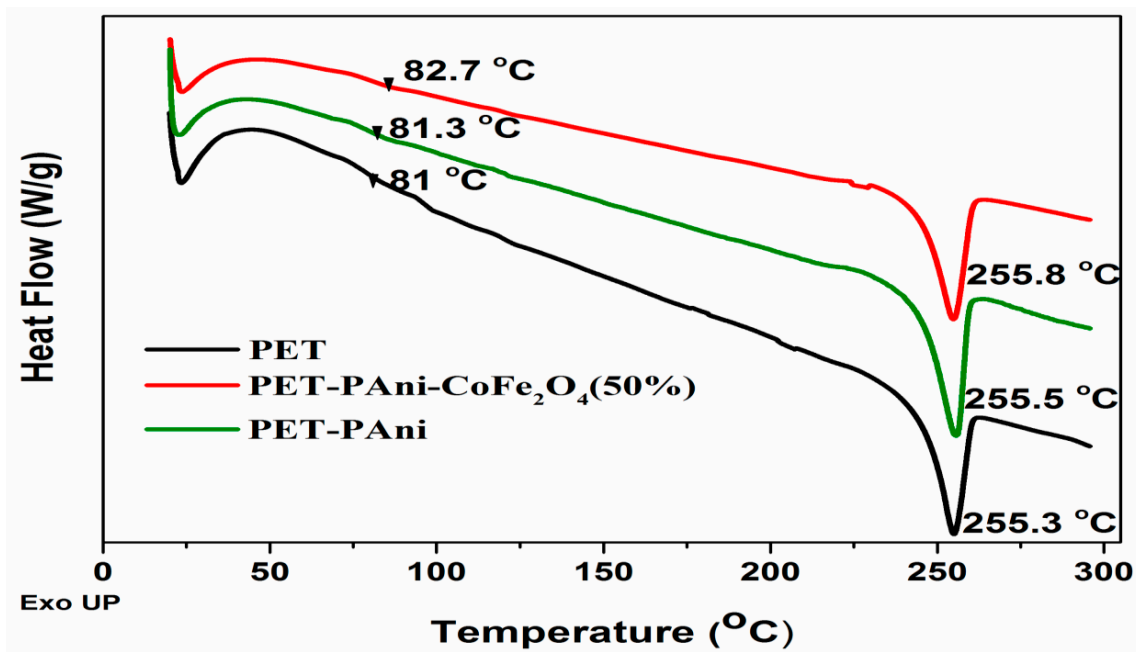


Figure 10. DSC thermograms of PET, PET-PANi and PET-PANi-CoFe₂O₄ (50%).

3.8. XPS Spectra

The chemical composition and the oxidation state of PANi-CoFe₂O₄ (50%) nanocomposite was elucidated by XPS measurements (Figure 11). The XPS spectrum confirms the presence of Co, Fe, N, O and C in the nanocomposite, Figure 11a. The core level of C1s (Figure 11b) deconvoluted into four distinct peaks at 283.8 eV, 284.7 eV and 287.3 eV, which belongs to —C=C, C—N, and C=O bands, respectively [51,52]. The peak at 285.7 eV is related to C—O [53]. Figure 11c shows the N1s' core level and they fit well into three peaks located at 398.8 eV, 400.5 eV and 402.6 eV that can be attributed to quinoid imine (—N=), benzenoid amine (—NH—) and (N⁺) of PANi chain, respectively [54]. At lower binding energy, there are two peaks situated at 529.6 and 532 eV for O1s, Figure 11d. The peak at 529.6 eV confirms Co—O, while the peak at 532 eV is attributed to (OH) group and

defect sites of oxygen [55]. In Figure 11e, the main peak Fe 2p_{3/2}, with a satellite peak at 716.8 eV, is fitted into two peaks of Fe 2p_{3/2} and Fe 2p_{1/2} at binding energies 710.5 and 712.7, respectively. These peaks indicate the presence of Fe species in two different lattice positions, the peak at 710.3 eV from Fe³⁺ ions in octahedral sites while the peak at 712.7 eV from Fe³⁺ ions in tetrahedral sites [56]. Figure 11f shows two major peaks which can be attributed to Co 2p_{3/2} at 780 eV and Co 2p_{1/2} at 796.1 eV. Where Co 2p_{3/2} is well fitted into two peaks, at 779.8 eV for Co²⁺ in octahedral sites and 781.5 eV for Co²⁺ in tetrahedral sites with satellite peak at 786 eV, while Co 2p_{1/2} is well fitted into one peak at 796.2 eV for Co²⁺ in octahedral sites with satellite peak at 803.2 eV [57]. Thus, the analysis of XPS confirms the PAni-CoFe₂O₄ (50%) nanocomposite formation.

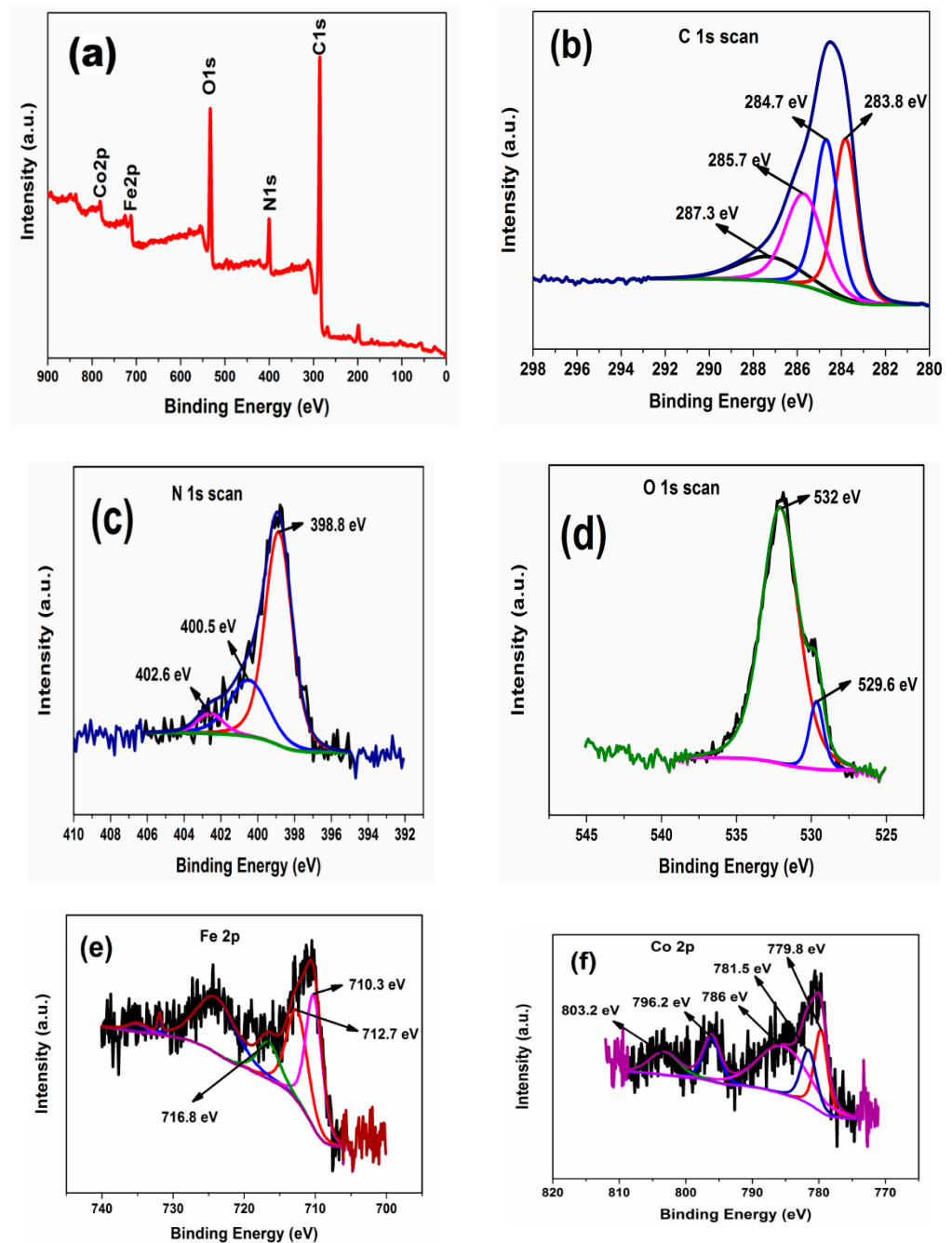


Figure 11. XPS of PAni-CoFe₂O₄ (50%) nanocomposite: (a) survey spectra, (b) C1s spectra, (c) N1s spectra, (d) O1s spectra, (e) Fe 2p, (f) Co 2p.

3.9. Gas Sensing Measurements

3.9.1. Selectivity of PET-PAni-CoFe₂O₄ Film

Gas sensing selectivity is a critical parameter for evaluation any chemi-resistive gas sensor performance. Different gases were used to test the selectivity of PET-PAni-CoFe₂O₄ flexible film at 50 ppm of each gas and the bar charts of selectivity towards NH₃, CO₂, methanol and ethanol are shown in Figure 12a. The study clearly demonstrates the selectivity of the PET-PAni and PET-PAni-CoFe₂O₄ flexible films for NH₃ compared to other gases. This selectivity may be due to the intense interactions between the sensing layers of flexible films and the adsorbed molecules of NH₃ gas. Moreover, the PET-PAni-CoFe₂O₄ (50%) showed the highest value of response (118.3%) towards 50 ppm of NH₃ compared to PET-PAni (10.16%). The response using the PET-PAni-CoFe₂O₄ (10%) of PET-PAni-CoFe₂O₄ was found to be 30.12% while it was 56.6% for the PET-PAni-CoFe₂O₄ (30%) (Figure 12b). The higher response value at PET-PAni-CoFe₂O₄ (50%) is mainly attributed to the porous structure [58], as noticed by FE-SEM. Hence, the PET-PAni-CoFe₂O₄ (50%) was selected for further analysis of its selectivity at room temperature sensing of NH₃ gas.

3.9.2. Response-Dependent Characteristics of PET-PAni-CoFe₂O₄ (50%) Film

The gas response time-dependent profile of PET-PAni-CoFe₂O₄ (50%) sensor towards 1–50 ppm of NH₃ is shown in Figure 12c. The dynamic response profile revealed that the flexible sensor is sensitive to 1 ppm NH₃ concentration with response of (6.1%). Moreover, the increase in NH₃ gas concentration led to an increase in the sensor response that reaches its maximum response of 118.3% at 50 ppm NH₃ gas. At higher NH₃ concentration, the molecules of gas cover the sensor active sites and involved in surface interactions giving even higher response. Additionally, the relative humidity (RH) effect on the NH₃ gas sensing of the PET-PAni-CoFe₂O₄ (50%) sensor was monitored for 50 ppm NH₃ at different RH, and data is plotted in Figure 12d. The PET-PAni-CoFe₂O₄ (50%) sensor displayed a maximum response value of 124.8% at 20% RH, while the response decreased to 118.3% at 40% RH. Further increase in RH leads to a decrease in the sensor response, hence, the response is greatly affected by RH. Obviously, when the sensor film is subjected to high concentrations of RH, the molecules of water occupy some active sites of the sensor and overlap with the adsorbed molecules of the target gas that is probably reason of reduced response at higher RH [59,60]. The resistance dynamic change of PET-PAni-CoFe₂O₄ (50%) sensor when exposed to different concentrations of NH₃ gas (1–50 ppm) is shown in Figure 12e.

3.9.3. Reproducibility, Response-Recovery Times and Flexibility of the Sensor

The reproducibility and stability of the sensor are imperative characteristics to show its reliability. The reproducibility of PET-PAni-CoFe₂O₄ (50%) sensor was evaluated by repeating the exposure cycles for four times at 10 ppm NH₃ and the response values are shown in Figure 13a. The PET-PAni-CoFe₂O₄ (50%) response is almost the same for four cycles. Thus, PET-PAni-CoFe₂O₄ (50%) sensor has excellent reproducibility and can be utilized repetitively for the room temperature and lower concentration detection of NH₃ gas.

Figure 13b represents the times of response and recovery, which are measured from the dynamic response curves of PET-PAni-CoFe₂O₄ (50%) sensor at different gas concentrations shown in Figure 12c. The response and recovery times were inversely changed with NH₃ gas concentrations, the sensor at 50 ppm of NH₃ gas showed lowest response time (24.3 s). The effect is due to large availability of porous sites on the surface of the sensor for adsorption of gas requiring a short response time while the recovery time increased due to decrease in reactive species desorption rate after NH₃ gas removal [58]. Furthermore, the response of PET-PAni-CoFe₂O₄ (50%) sensor toward very low NH₃ concentrations (25–100 ppb) has also been evaluated and the response curve is shown in Figure 13c. It is clear that the developed PET-PAni-CoFe₂O₄ (50%) sensor is very sensitive to low concentrations and practically can detect as low as 25 ppb of NH₃ gas that effectively meets

the requirement of health and environmental issues. The flexibility of PET-PAni-CoFe₂O₄ (50%) sensor was evaluated after 500 bending cycles at 50 ppm NH₃ and data is displayed in Figure 13d. An insignificant change in the sensor response (from 118.3% to 114.9%) is observed, indicating the excellent stability of PET-PAni-CoFe₂O₄ (50%) sensor after repeated cycles of bending.

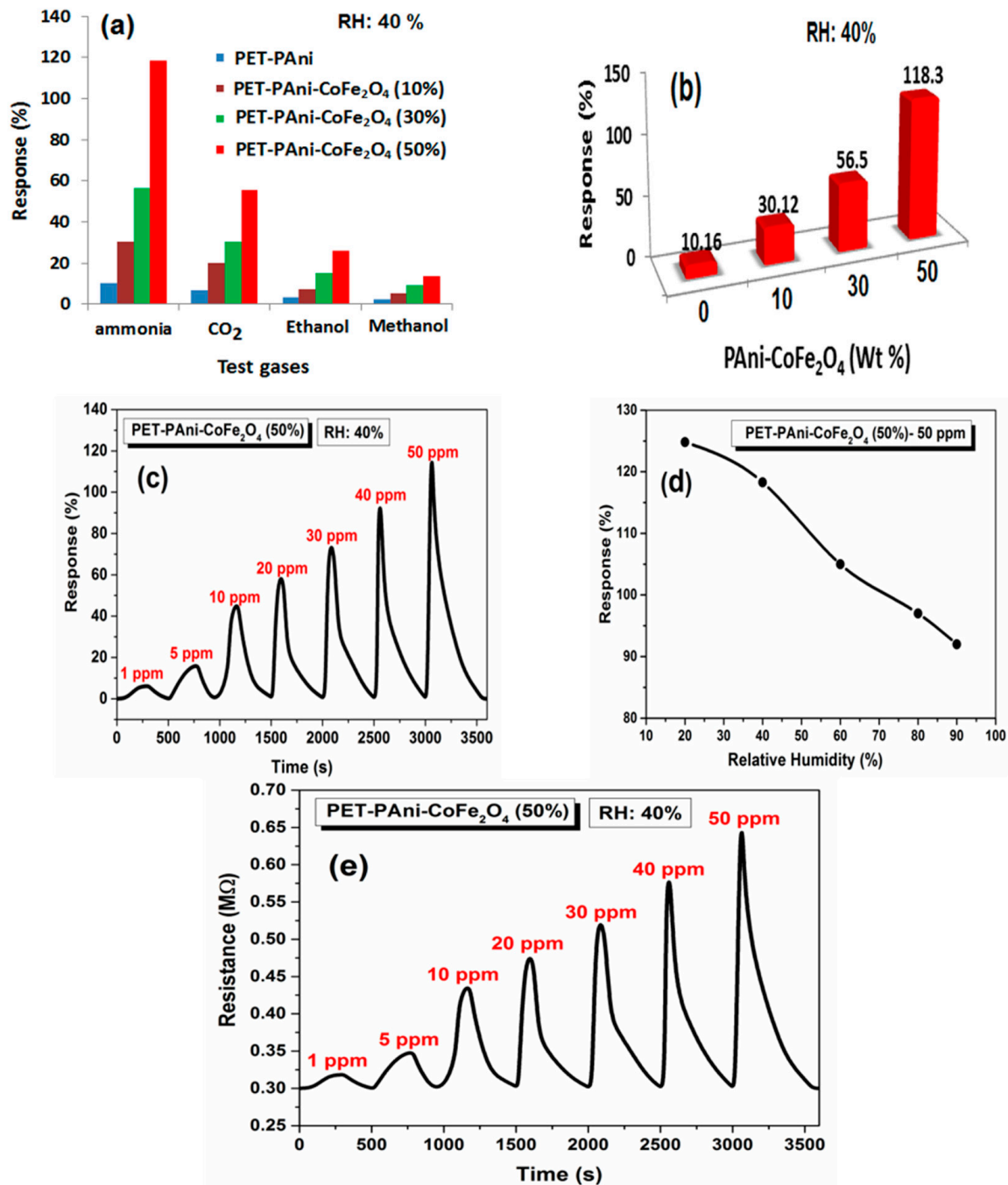


Figure 12. (a) Selectivity of PET-PAni and PET-PAni-CoFe₂O₄ films towards different test gases at 50 ppm, (b) Response of PET-PAni and PET-PAni-CoFe₂O₄ films towards 50 ppm NH₃ gas, (c) Response of PET-PAni-CoFe₂O₄ (50%) to 1–50 ppm of NH₃, (d) Humidity study of PET-PAni-CoFe₂O₄ (50%) at 50 ppm NH₃ gas and (e) Resistance values of PET-PAni-CoFe₂O₄ (50%) to 1–50 ppm of NH₃.

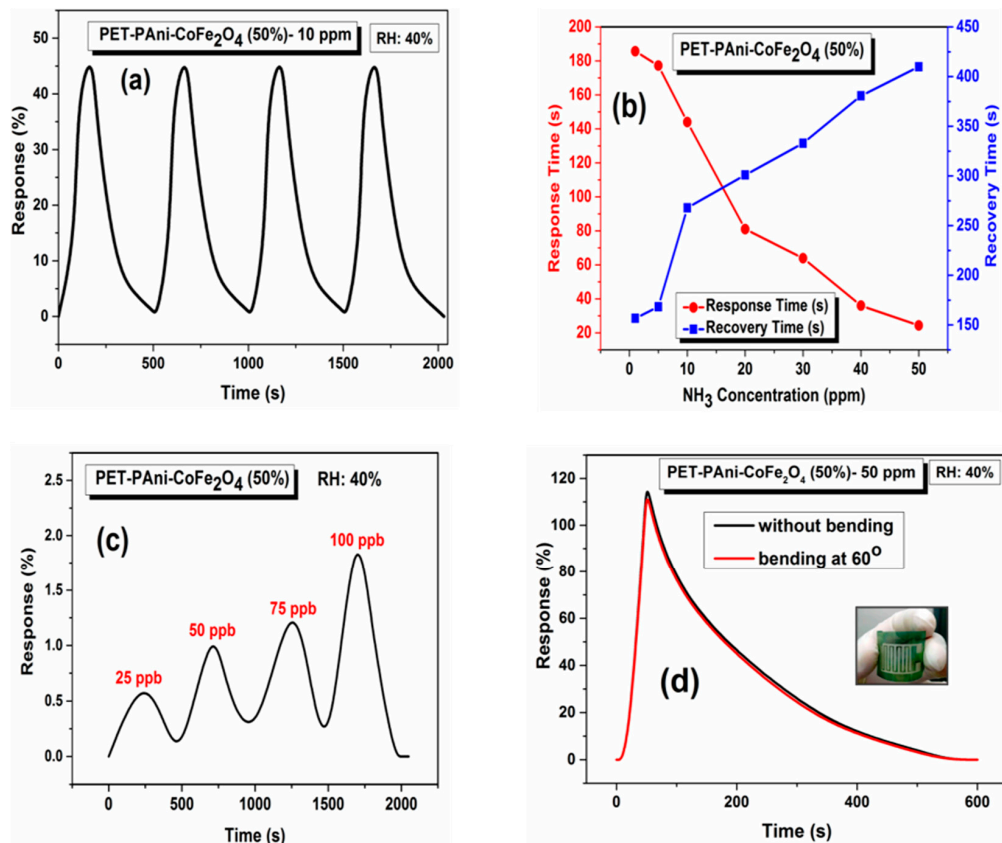


Figure 13. (a) Reproducibility of PET-PAni-CoFe₂O₄ (50%) to 10 ppm of NH₃ gas, (b) Response and recovery time of PET-PAni-CoFe₂O₄ (50%) sensor, (c) detection limit of PET-PAni-CoFe₂O₄ (50%), (d) flexibility of PET-PAni-CoFe₂O₄ (50%) at bending angle 60° at 50 ppm of NH₃ gas.

There are several reports in the literature for NH₃ sensors. A comparison of the sensing performance of PET-PAni-CoFe₂O₄ (50%) developed in current study with the reported method is presented in Table 1. The PET-PAni-CoFe₂O₄ (50%) sensor developed in this study exhibits ultra-low detection limit, high response, and excellent flexibility, which shows its potential to be used in the portable NH₃ sensing device development.

Table 1. The sensing properties comparison of PET-PAni-CoFe₂O₄ (50%) with other reported works.

Material	Substrate	Detection Limit	Response %	Response Time (s)	Flexibility	Ref.
PAni	PET	<5 ppm	26 (100 ppm)	33	-	[61]
S, N: GQDs/PAni	PET	1 ppm	42.3 (100 ppm)	115	The response at bending angle 80° was more than at 0°	[14]
MWCNT-PAni	PVDF	0.1 ppm	32 (1 ppm)	76	Less than 10% deviation after 500 bending cycles @ 60°	[11]
PAni-α-Fe ₂ O ₃	PET	<2.5 ppm	72 (100 ppm)	50	-	[62]
GP-PAni	PVDF	100 ppb	60 (1 ppm)	46	The response decreased from 60 to 49% at 1500 bending cycles	[4]
PAni-WO ₃	PET	1 ppm	121 (100 ppm)	32	the response decreased by 9% @ 60° bending, 900 s	[58]
MWCNTs-PAni	Modified PET	33 ppm	117 (50 ppm)	47	-	[19]
PPy	silk	1 ppm	73.25 (100 ppm)	24	The response decreased by 10.61% @ 30° after 200 bending cycles	[63]
PAni-CoFe ₂ O ₄	PET	25 ppb	118.3 (50 ppm)	24.3	Stable response after 500 bending cycle with 3.4% decrease @ 60°	This work

3.9.4. Proposed Mechanism of Gas Sensing

Protonation and deprotonation phenomenon resulting from NH_3 gas adsorption and desorption is responsible for the response in pure PANi sensor. When NH_3 gas is introduced to the sensor surface, the PANi emeraldine salt (ES) is converted to PANi emeraldine base (EB). Consequently, the PANi hole density decreases which leads to an increase in the resistance [64,65]. The gas sensing in the nanocomposite film predominantly depends on NH_3 gas trapping that leads to the change in resistance. Figure 14 shows the schematic sensing model of PANi- CoFe_2O_4 flexible sensor at ambient. The n-type CoFe_2O_4 NPs were wrapped in the p-type PANi emeraldine salt to obtain porous nanocomposite due to integration of CoFe_2O_4 in the PANi matrix as observed in FE-SEM images which leads to formation active centers on the film surface with donor and acceptor states. Thus, it could be concluded that the p-n junctions are established at PANi- CoFe_2O_4 interface. When the sensor film is exposed to NH_3 , the molecules of gas would capture holes from $-\text{NH}_2-$ and $=\text{NH}^+$ groups of PANi [66] and converts from emeraldine salt to emeraldine base as shown in Figure 14a, resulting in a decrease in PANi conductivity [14]. The adsorption of NH_3 as a reducing gas leads to decrease in the concentration of PANi holes and p-n junctions depletion regions are widened as shown in shown in Figure 14b. The interaction between NH_3 gas released free electrons, and hence neutralize the holes found on PANi surface due to electron-hole combination. This leads to a decrease in the concentration of hole and heterojunctions, as a result resistance of the nanocomposite sensor increases.

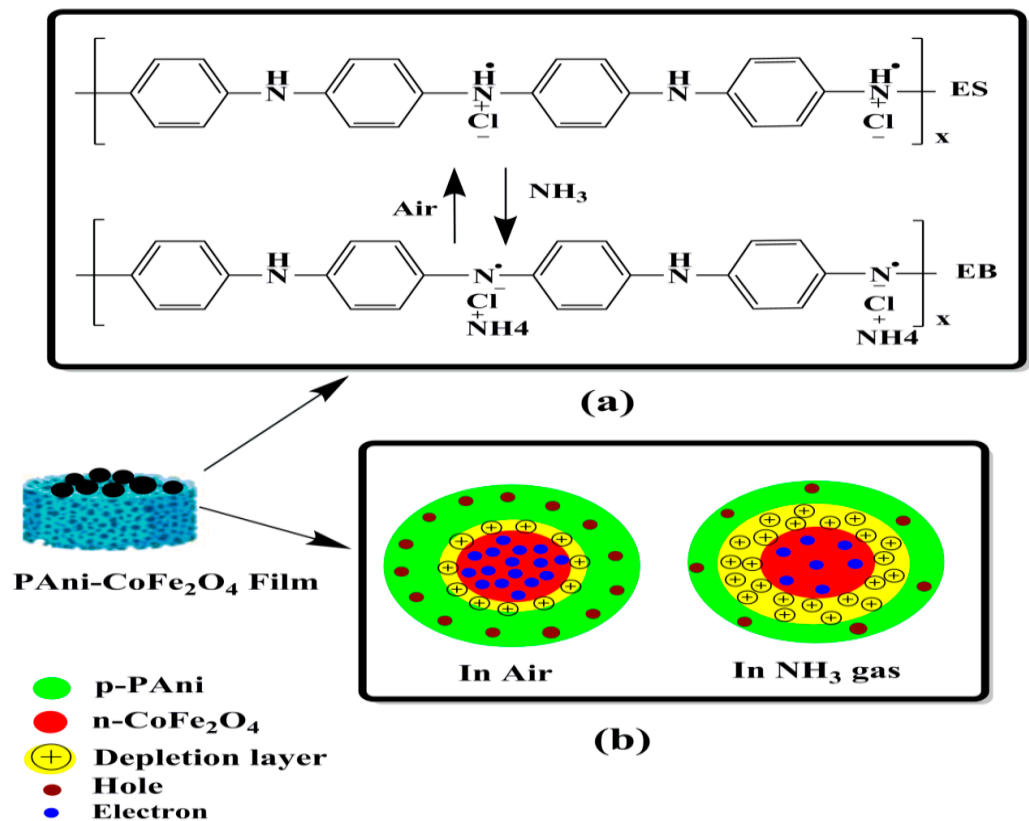


Figure 14. Schematic sensing model of PANi- CoFe_2O_4 flexible sensor, (a) the NH_3 gas interaction with the PANi emeraldine salt, and (b) the depletion region changes of PET-PANi- CoFe_2O_4 in air and NH_3 gas.

4. Conclusions

In the present work, a flexible gas sensor composed of a thin film of PANi-CoFe₂O₄ nanocomposites on PET substrate by using simple in situ chemical oxidative polymerization technique with different CoFe₂O₄ NPs concentrations is reported. The developed sensor is subsequently applied successfully for room temperature NH₃ gas sensing. The morphological analyses reveal porous structure the PANi-CoFe₂O₄ flexible film. The formation of PANi-CoFe₂O₄ nanocomposites confirmed by XPS analysis. The gas sensing data showed that the PET-PANi and PET-PANi-CoFe₂O₄ sensors have highest values of selectivity when exposed to NH₃ gas at room temperature compared to other environmental gases. The PET-PANi-CoFe₂O₄ (50%) flexible sensor demonstrated a maximum response value of 118.3%, excellent response time of (24.3 s) at 50 ppm NH₃ gas. The sensor has good reproducibility, ultra-low detection limit (25 ppb) and excellent flexibility with insignificant response change after repeated cycles of process and bending. Therefore, this paper highlights that the as-fabricated flexible PET-PANi-CoFe₂O₄ (50%) sensor provides a promising platform for trace-level NH₃ detection of NH₃ gas on chemicals production field and environmental testing.

Author Contributions: Conceptualization, methodology, validation, investigation, formal analysis, data curation, writing—original draft preparation, R.D.A. and A.S. All authors have read and agreed to the published version of the manuscript.

Funding: This Project was funded by the Deanship of Scientific Research (DSR), King Abdulaziz University, Jeddah, under grant No (G:120-665-1441). The authors, therefore, acknowledge with thanks DSR technical and financial support.

Institutional Review Board Statement: Not Applicable.

Informed Consent Statement: Not Applicable.

Data Availability Statement: Not Applicable.

Acknowledgments: The authors want to thank the reviewers for their informative comments and advice that did improve the paper markedly.

Conflicts of Interest: The authors declare no conflict of interest.

References

1. Zhang, J.; Ouyang, J.; Ye, Y.; Li, Z.; Lin, Q.; Chen, T.; Zhang, Z.; Xiang, S. Mixed-valence cobalt (II/III) metal–organic framework for ammonia sensing with naked-eye color switching. *ACS Appl. Mater. Interfaces* **2018**, *10*, 27465–27471. [[CrossRef](#)]
2. Wongchoosuk, C.; Jangtaewee, P.; Lokavee, P.; Udomrat, S.; Sudkeaw, P.; Kerdcharoen, T. Novel flexible NH₃ gas sensor prepared by ink-jet printing technique. In *Advanced Materials Research*; Trans Tech Publications Ltd.: Bäch, Switzerland, 2012; Volume 506, pp. 39–42.
3. Maity, D.; Kumar, R.T.R. Polyaniline anchored MWCNTs on fabric for high performance wearable ammonia sensor. *ACS Sens.* **2018**, *3*, 1822–1830. [[CrossRef](#)] [[PubMed](#)]
4. Wu, Q.; Shen, W.; Lv, D.; Chen, W.; Song, W.; Tan, R. An enhanced flexible room temperature ammonia gas sensor based on GP-PANI/PVDF multi-hierarchical nanocomposite film. *Sens. Actuators B Chem.* **2021**, *334*, 129630. [[CrossRef](#)]
5. Moghaddam, H.M.; Malkeshi, H. Self-assembly synthesis and ammonia gas-sensing properties of ZnO/Polythiophene nanofibers. *J. Mater. Sci. Mater. Electron.* **2016**, *27*, 8807–8815. [[CrossRef](#)]
6. Jia, X.-S.; Tang, C.-C.; Yan, X.; Yu, G.-F.; Li, J.-T.; Zhang, H.-D.; Li, J.-J.; Gu, C.-Z.; Long, Y.-Z. Flexible polyaniline/poly (methyl methacrylate) composite fibers via electrospinning and in situ polymerization for ammonia gas sensing and strain sensing. *J. Nanomater.* **2016**, *2016*. [[CrossRef](#)]
7. Su, P.-G.; Lee, C.-T.; Chou, C.-Y. Flexible NH₃ sensors fabricated by in situ self-assembly of polypyrrole. *Talanta* **2009**, *80*, 763–769. [[CrossRef](#)] [[PubMed](#)]
8. Bittencourt, J.C.; de Santana Gois, B.H.; Rodrigues de Oliveira, V.J.; da Silva Agostini, D.L.; de Almeida Olivati, C. Gas sensor for ammonia detection based on poly (vinyl alcohol) and polyaniline electrospun. *J. Appl. Polym. Sci.* **2019**, *136*, 47288. [[CrossRef](#)]
9. Eising, M.; Cava, C.E.; Salvatierra, R.V.; Zarbin, A.J.G.; Roman, L.S. Doping effect on self-assembled films of polyaniline and carbon nanotube applied as ammonia gas sensor. *Sens. Actuators B Chem.* **2017**, *245*, 25–33. [[CrossRef](#)]
10. Wu, J.; Zhang, Q.; Zhou, A.; Huang, Z.; Bai, H.; Li, L. Phase-separated polyaniline/graphene composite electrodes for high-rate electrochemical supercapacitors. *Adv. Mater.* **2016**, *28*, 10211–10216. [[CrossRef](#)]

11. Wu, T.; Lv, D.; Shen, W.; Song, W.; Tan, R. Trace-level ammonia detection at room temperature based on porous flexible polyaniline/polyvinylidene fluoride sensing film with carbon nanotube additives. *Sens. Actuators B Chem.* **2020**, *316*, 128198. [[CrossRef](#)]
12. Bandgar, D.K.; Navale, S.T.; Naushad, M.; Mane, R.S.; Stadler, F.J.; Patil, V.B. Ultra-sensitive polyaniline-iron oxide nanocomposite room temperature flexible ammonia sensor. *RSC Adv.* **2015**, *5*, 68964–68971. [[CrossRef](#)]
13. Shrivastav, A.M.; Sharma, G.; Rathore, A.S.; Jha, R. Hypersensitive and selective interferometric nose for ultratrace ammonia detection with fast response utilizing PANI@SnO₂ nanocomposite. *ACS Photonics* **2018**, *5*, 4402–4412. [[CrossRef](#)]
14. Gavvani, J.N.; Hasani, A.; Nouri, M.; Mahyari, M.; Salehi, A. Highly sensitive and flexible ammonia sensor based on S and N co-doped graphene quantum dots/polyaniline hybrid at room temperature. *Sens. Actuators B Chem.* **2016**, *229*, 239–248. [[CrossRef](#)]
15. Liu, C.; Tai, H.; Zhang, P.; Yuan, Z.; Du, X.; Xie, G.; Jiang, Y. A high-performance flexible gas sensor based on self-assembled PANI-CeO₂ nanocomposite thin film for trace-level NH₃ detection at room temperature. *Sens. Actuators B Chem.* **2018**, *261*, 587–597. [[CrossRef](#)]
16. Su, P.-G.; Liao, Z.-H. Fabrication of a flexible single-yarn NH₃ gas sensor by layer-by-layer self-assembly of graphene oxide. *Mater. Chem. Phys.* **2019**, *224*, 349–356. [[CrossRef](#)]
17. Feng, Q.; Zhang, H.; Shi, Y.; Yu, X.; Lan, G. Preparation and Gas Sensing Properties of PANI/SnO₂ Hybrid Material. *Polymers* **2021**, *13*, 1360. [[CrossRef](#)]
18. Zhang, Y.; Zhang, J.; Jiang, Y.; Duan, Z.; Liu, B.; Zhao, Q.; Wang, S.; Yuan, Z.; Tai, H. Ultrasensitive flexible NH₃ gas sensor based on polyaniline/SrGe₄O₉ nanocomposite with ppt-level detection ability at room temperature. *Sens. Actuators B Chem.* **2020**, *319*, 128293. [[CrossRef](#)]
19. Ma, J.; Fan, H.; Li, Z.; Jia, Y.; Yadav, A.K.; Dong, G.; Wang, W.; Dong, W.; Wang, S. Multi-walled carbon nanotubes/polyaniline on the ethylenediamine modified polyethylene terephthalate fibers for a flexible room temperature ammonia gas sensor with high responses. *Sens. Actuators B Chem.* **2021**, *334*, 129677. [[CrossRef](#)]
20. Dutta, V.; Sharma, S.; Raizada, P.; Hosseini-Bandegharai, A.; Gupta, V.K.; Singh, P. Review on augmentation in photocatalytic activity of CoFe₂O₄ via heterojunction formation for photocatalysis of organic pollutants in water. *J. Saudi Chem. Soc.* **2019**, *23*, 1119–1136.
21. Kim, W.C.; Lee, S.W.; Kim, S.J.; Yoon, S.H.; Kim, C.S. Magnetic properties of Y-, La-, Nd-, Gd-, and Bi-doped ultrafine CoFe₂O₄ spinel grown by using a sol-gel method. *J. Magn. Magn. Mater.* **2000**, *215*, 217–220. [[CrossRef](#)]
22. Torkian, S.; Ghasemi, A.; Razavi, R.S. Cation distribution and magnetic analysis of wideband microwave absorptive Co_xNi_{1-x}Fe₂O₄ ferrites. *Ceram. Int.* **2017**, *43*, 6987–6995. [[CrossRef](#)]
23. Li, X.-H.; Xu, C.-L.; Han, X.-H.; Qiao, L.; Wang, T.; Li, F.-S. Synthesis and magnetic properties of nearly monodisperse CoFe₂O₄ nanoparticles through a simple hydrothermal condition. *Nanoscale Res. Lett.* **2010**, *5*, 1039–1044. [[CrossRef](#)]
24. Prasad, P.D.; Hemalatha, J. Enhanced magnetic properties of highly crystalline cobalt ferrite fibers and their application as gas sensors. *J. Magn. Magn. Mater.* **2019**, *484*, 225–233. [[CrossRef](#)]
25. Bagade, A.A.; Ganbavle, V.V.; Mohite, S.V.; Dongale, T.D.; Sinha, B.B.; Rajpure, K.Y. Assessment of structural, morphological, magnetic and gas sensing properties of CoFe₂O₄ thin films. *J. Colloid Interface Sci.* **2017**, *497*, 181–192. [[CrossRef](#)]
26. Caldeira, L.E.; Guaglianoni, W.C.; Venturini, J.; Arcaro, S.; Bergmann, C.P.; Bragança, S.R. Sintering-dependent mechanical and magnetic properties of spinel cobalt ferrite (CoFe₂O₄) ceramics prepared via sol-gel synthesis. *Ceram. Int.* **2020**, *46*, 2465–2472. [[CrossRef](#)]
27. Zeng, W.; Li, Y.; Miao, B.; Lin, L.; Wang, Z. Recognition of carbon monoxide with SnO₂/Ti thick-film sensor and its gas-sensing mechanism. *Sens. Actuators B Chem.* **2014**, *191*, 1–8. [[CrossRef](#)]
28. Wang, J.; Zeng, W.; Wang, Z. Assembly of 2D nanosheets into 3D flower-like NiO: Synthesis and the influence of petal thickness on gas-sensing properties. *Ceram. Int.* **2016**, *42*, 4567–4573. [[CrossRef](#)]
29. Guo, W.; Fu, M.; Zhai, C.; Wang, Z. Hydrothermal synthesis and gas-sensing properties of ultrathin hexagonal ZnO nanosheets. *Ceram. Int.* **2014**, *40*, 2295–2298. [[CrossRef](#)]
30. Zeng, W.; Zhang, H.; Wang, Z. Effects of different petal thickness on gas sensing properties of flower-like WO₃·H₂O hierarchical architectures. *Appl. Surf. Sci.* **2015**, *347*, 73–78. [[CrossRef](#)]
31. Gonzalez-Sandoval, M.P.; Beesley, A.M.; Miki-Yoshida, M.; Fuentes-Cobas, L.; Matutes-Aquino, J.A. Comparative study of the microstructural and magnetic properties of spinel ferrites obtained by co-precipitation. *J. Alloys Compd.* **2004**, *369*, 190–194. [[CrossRef](#)]
32. Geng, L.; Zhao, Y.; Huang, X.; Wang, S.; Zhang, S.; Wu, S. Characterization and gas sensitivity study of polyaniline/SnO₂ hybrid material prepared by hydrothermal route. *Sens. Actuators B Chem.* **2007**, *120*, 568–572. [[CrossRef](#)]
33. Youssef, A.M.; Mohamed, S.A.; Abdel-Aziz, M.S.; Abdel-Aziz, M.E.; Turkey, G.; Kamel, S. Biological studies and electrical conductivity of paper sheet based on PANI/PS/Ag-NPs nanocomposite. *Carbohydr. Polym.* **2016**, *147*, 333–343. [[CrossRef](#)]
34. Vivekanandan, J.; Ponnusamy, V.; Mahudewaran, A.; Vijayanand, P.S. Synthesis, characterization and conductivity study of polyaniline prepared by chemical oxidative and electrochemical methods. *Arch. Appl. Sci. Res.* **2011**, *3*, 147–153.
35. Mu, B.; Zhang, W.; Shao, S.; Wang, A. Glycol assisted synthesis of graphene-MnO₂-polyaniline ternary composites for high performance supercapacitor electrodes. *Phys. Chem. Chem. Phys.* **2014**, *16*, 7872–7880. [[CrossRef](#)] [[PubMed](#)]

36. Muthukumar, T.; Philip, J. A facile approach to synthesis of cobalt ferrite nanoparticles with a uniform ultrathin layer of silicon carbide for organic dye removal. *J. Mol. Liq.* **2020**, *317*, 114110. [[CrossRef](#)]
37. Abdel-Aziz, M.H.; Zoromba, M.S.; Bassyouni, M.; Zwawi, M.; Alshehri, A.A.; Al-Hossainy, A.F. Synthesis and characterization of Co-Al mixed oxide nanoparticles via thermal decomposition route of layered double hydroxide. *J. Mol. Struct.* **2020**, *1206*, 127679. [[CrossRef](#)]
38. Trad, T.M.; Alvarez, R.M.; McCumiskey, E.J.; Taylor, C.R. Capped CoFe₂O₄ Nanoparticles: Non-Hydrolytic Synthesis, Characterization, and Potential Applications as Magnetic Extractants and in Ferrofluids. *Adv. Nanomater. Nanostructures* **2011**, *229*, 155–162.
39. He, K.; Li, M.; Guo, L. Preparation and photocatalytic activity of PANI-CdS composites for hydrogen evolution. *Int. J. Hydrogen Energy* **2012**, *37*, 755–759. [[CrossRef](#)]
40. Li, X.; Wang, D.; Cheng, G.; Luo, Q.; An, J.; Wang, Y. Preparation of polyaniline-modified TiO₂ nanoparticles and their photocatalytic activity under visible light illumination. *Appl. Catal. B Environ.* **2008**, *81*, 267–273. [[CrossRef](#)]
41. Kim, K.N.; Jung, H.-R.; Lee, W.-J. Hollow cobalt ferrite–polyaniline nanofibers as magnetically separable visible-light photocatalyst for photodegradation of methyl orange. *J. Photochem. Photobiol. A Chem.* **2016**, *321*, 257–265. [[CrossRef](#)]
42. Šuljagić, M.; Vulić, P.; Jeremić, D.; Pavlović, V.; Filipović, S.; Kilanski, L.; Lewinska, S.; Slawska-Waniewska, A.; Milenković, M.R.; Nikolić, A.S. The influence of the starch coating on the magnetic properties of nanosized cobalt ferrites obtained by different synthetic methods. *Mater. Res. Bull.* **2021**, *134*, 111117. [[CrossRef](#)]
43. Abou Hammad, A.B.; Abd El-Aziz, M.E.; Hasanin, M.S.; Kamel, S. A novel electromagnetic biodegradable nanocomposite based on cellulose, polyaniline, and cobalt ferrite nanoparticles. *Carbohydr. Polym.* **2019**, *216*, 54–62. [[CrossRef](#)]
44. Kaur, H.; Singh, A.; Kumar, V.; Ahlawat, D.S. Structural, thermal and magnetic investigations of cobalt ferrite doped with Zn²⁺ and Cd²⁺ synthesized by auto combustion method. *J. Magn. Magn. Mater.* **2019**, *474*, 505–511. [[CrossRef](#)]
45. Bhadra, J.; Al-Thani, N.J.; Madi, N.K.; Al-Maadeed, M.A. Effects of aniline concentrations on the electrical and mechanical properties of polyaniline polyvinyl alcohol blends. *Arab. J. Chem.* **2017**, *10*, 664–672. [[CrossRef](#)]
46. Islam, M.S.; Miran, M.S.; Rahman, M.M.; Mollah, M.Y.A.; Susan, M. Polyaniline-silica composite materials: Influence of silica content on the thermal and thermodynamic properties. *J. Nanostruct. Polym. Nanocompos.* **2013**, *9*, 83–89.
47. Abdel-Galil, E.A.; Tourky, A.S.; Kasem, A.E. Sorption of some radionuclides from nuclear waste effluents by polyaniline/SiO₂ composite: Characterization, thermal stability, and gamma irradiation studies. *Appl. Radiat. Isot.* **2020**, *156*, 109009. [[CrossRef](#)] [[PubMed](#)]
48. Nisticò, R. Polyethylene terephthalate (PET) in the packaging industry. *Polym. Test.* **2020**, *90*, 106707. [[CrossRef](#)]
49. Wolinska-Grabczyk, A.; Kubica, P.; Jankowski, A. Effect of the acetate group content on gas permeation through membranes based on poly (ethylene-co-vinyl acetate) and its blends. *J. Memb. Sci.* **2013**, *443*, 227–236. [[CrossRef](#)]
50. Özen, İ.; Bozoklu, G.; Dalgıçdir, C.; Yücel, O.; Ünsal, E.; Çakmak, M.; Menceloğlu, Y.Z. Improvement in gas permeability of biaxially stretched PET films blended with high barrier polymers: The role of chemistry and processing conditions. *Eur. Polym. J.* **2010**, *46*, 226–237. [[CrossRef](#)]
51. Han, M.G.; Im, S.S. X-ray photoelectron spectroscopy study of electrically conducting polyaniline/polyimide blends. *Polymer* **2000**, *41*, 3253–3262. [[CrossRef](#)]
52. Mohamed, S.G.; Attia, S.Y.; Barakat, Y.F.; Hassan, H.H.; Zoubi, W. Al Hydrothermal synthesis of α-MnS nanoflakes@ nitrogen and sulfur Co-doped rGO for high-performance hybrid supercapacitor. *ChemistrySelect* **2018**, *3*, 6061–6072. [[CrossRef](#)]
53. Zha, D.; Xiong, P.; Wang, X. Strongly coupled manganese ferrite/carbon black/polyaniline hybrid for low-cost supercapacitors with high rate capability. *Electrochim. Acta* **2015**, *185*, 218–228. [[CrossRef](#)]
54. Kim, M.; Lee, C.; Jang, J. Fabrication of highly flexible, scalable, and high-performance supercapacitors using polyaniline/reduced graphene oxide film with enhanced electrical conductivity and crystallinity. *Adv. Funct. Mater.* **2014**, *24*, 2489–2499. [[CrossRef](#)]
55. Mohamed, S.G.; Attia, S.Y.; Hassan, H.H. Spinel-structured FeCo₂O₄ mesoporous nanosheets as efficient electrode for supercapacitor applications. *Microporous Mesoporous Mater.* **2017**, *251*, 26–33. [[CrossRef](#)]
56. WP, W.; Yang, H.; Xian, T.; JL, J. XPS and magnetic properties of CoFe₂O₄ nanoparticles synthesized by a polyacrylamide gel route. *Mater. Trans.* **2012**, *53*, 1586–1589.
57. Fantauzzi, M.; Secci, F.; Angotzi, M.S.; Passiu, C.; Cannas, C.; Rossi, A. Nanostructured spinel cobalt ferrites: Fe and Co chemical state, cation distribution and size effects by X-ray photoelectron spectroscopy. *RSC Adv.* **2019**, *9*, 19171–19179. [[CrossRef](#)]
58. Kulkarni, S.B.; Navale, Y.H.; Navale, S.T.; Stadler, F.J.; Ramgir, N.S.; Patil, V.B. Hybrid polyaniline-WO₃ flexible sensor: A room temperature competence towards NH₃ gas. *Sens. Actuators B Chem.* **2019**, *288*, 279–288. [[CrossRef](#)]
59. Cho, J.-H.; Yu, J.-B.; Kim, J.-S.; Sohn, S.-O.; Lee, D.-D.; Huh, J.-S. Sensing behaviors of polypyrrole sensor under humidity condition. *Sens. Actuators B Chem.* **2005**, *108*, 389–392. [[CrossRef](#)]
60. Bissell, R.A.; Persaud, K.C.; Travers, P. The influence of non-specific molecular partitioning of analytes on the electrical responses of conducting organic polymer gas sensors. *Phys. Chem. Chem. Phys.* **2002**, *4*, 3482–3490. [[CrossRef](#)]
61. Bandgar, D.K.; Navale, S.T.; Nalage, S.R.; Mane, R.S.; Stadler, F.J.; Aswal, D.K.; Gupta, S.K.; Patil, V.B. Simple and low-temperature polyaniline-based flexible ammonia sensor: A step towards laboratory synthesis to economical device design. *J. Mater. Chem. C* **2015**, *3*, 9461–9468. [[CrossRef](#)]

62. Bandgar, D.K.; Navale, S.T.; Navale, Y.H.; Ingole, S.M.; Stadler, F.J.; Ramgir, N.; Aswal, D.K.; Gupta, S.K.; Mane, R.S.; Patil, V.B. Flexible camphor sulfonic acid-doped PANi/ α -Fe₂O₃ nanocomposite films and their room temperature ammonia sensing activity. *Mater. Chem. Phys.* **2017**, *189*, 191–197. [[CrossRef](#)]
63. She, C.; Li, G.; Zhang, W.; Xie, G.; Zhang, Y.; Li, L.; Yue, F.; Liu, S.; Jing, C.; Cheng, Y. A flexible polypyrrole/silk-fiber ammonia sensor assisted by silica nanosphere template. *Sens. Actuators A Phys.* **2021**, *317*, 112436. [[CrossRef](#)]
64. Li, Z.-F.; Blum, F.D.; Bertino, M.F.; Kim, C.-S.; Pillalamarri, S.K. One-step fabrication of a polyaniline nanofiber vapor sensor. *Sens. Actuators B Chem.* **2008**, *134*, 31–35. [[CrossRef](#)]
65. Arora, R.; Srivastav, A.; Mandal, U.K. Polyaniline Based Polymeric Nanocomposite Containing TiO₂ and SnO₂ for Environmental and Energy Applications. *Int. J. Mod. Eng. Res.* **2012**, *2*, 2384–2395.
66. Patil, U.V.; Ramgir, N.S.; Karmakar, N.; Bhogale, A.; Debnath, A.K.; Aswal, D.K.; Gupta, S.K.; Kothari, D.C. Room temperature ammonia sensor based on copper nanoparticle intercalated polyaniline nanocomposite thin films. *Appl. Surf. Sci.* **2015**, *339*, 69–74. [[CrossRef](#)]